

Design Study of a Multipole Ion Trap for Beam Physics Applications

Kei FUKUSHIMA and Hiromi OKAMOTO

Graduate School of Advanced Sciences of Matter, Hiroshima University, 1-3-1 Kagamiyama, Higashi-Hiroshima 739-8530, Japan

(Received 2 August 2015 / Accepted 3 September 2015)

A unique linear Paul trap is designed for a systematic experimental study of nonlinear beam dynamics with the tabletop apparatus “S-POD” at Hiroshima University. S-POD is the abbreviation of “Simulator of Particle Orbit Dynamics” where we can produce a non-neutral plasma physically equivalent to a charged-particle beam in an alternating-gradient focusing channel. Unlike a regular Paul trap with four quadrupole rods, the present trap configuration includes extra electrodes that enable us to control the strengths and time structures of low-order nonlinear fields independently of the linear focusing potential. We here consider the insertion of thin metallic plates in between the quadrupole rods. The size and arrangement of those extra electrodes are optimized by using a Poisson solver. Simple scaling laws are derived to make a quick estimate of the sextupole and octupole field strengths as a function of the plate dimension. Particle tracking simulations are performed to demonstrate the controlled excitation of nonlinear resonances in the modified Paul trap.

© 2015 The Japan Society of Plasma Science and Nuclear Fusion Research

Keywords: linear Paul trap, charged-particle beam dynamics, nonlinear resonance, application of non-neutral plasma

DOI: 10.1585/pfr.10.1401081

1. Introduction

The recent trend in advanced hadron accelerators makes it more important to understand the collective effect induced by the Coulomb self-field of a dense beam. This complex nonlinear phenomenon, generally referred to as *space-charge effect*, plays a crucial role in beam stability and, therefore, has to be carefully considered in choosing a proper operating condition of any high-intensity hadron machine [1–3]. Systematic experimental studies of space-charge-induced beam instabilities are, however, very difficult to conduct in practice due to many technical reasons. For instance, the lattice structure of an accelerator is not flexible, which limits the range of parameter space we can survey. We thus often employ multi-particle tracking codes to clarify how this type of instabilities depends on lattice designs, but high-precision numerical simulations are very time-consuming even with modern computers.

Although numerical simulations give us good insight into underlying physics, they cannot be substituted for experimental verification. At Hiroshima University, a unique tabletop tool called “S-POD” (Simulator of Particle Orbit Dynamics) has been developed which allows accelerator-free experiments on diverse beam-dynamics issues [4–10]. The S-POD system is based on a compact linear Paul trap in which we can confine a large number of ions¹. It is known that a non-neutral plasma stored in the trap can be made approximately equivalent to a charged-particle beam in an alternating-gradient (AG) transport channel [4].

Since S-POD has many practical advantages in exploring the fundamental aspects of beam dynamics, Rutherford Appleton Laboratory is now constructing essentially the same experimental apparatus in England².

The Paul trap is composed of four metallic rods symmetrically placed around the trap axis to provide a radio-frequency (rf) quadrupole field for transverse ion confinement [14]. The collective motion of confined ions obeys the Hamiltonian

$$H = \frac{p_x^2 + p_y^2}{2} + \frac{1}{2}K(\tau)(x^2 - y^2) + \delta V(x, y; \tau) + I_C \phi_{sc}(x, y; \tau), \quad (1)$$

where the independent variable has been scaled from time t to $\tau = ct$ with c being the speed of light, I_C is a constant that depends on the ion species, ϕ_{sc} is the scalar potential of the Coulomb self-field generated by the ions, and the function $K(\tau)$ is proportional to the rf voltage applied to the quadrupole rods. We here explicitly introduced the nonlinear perturbing potential δV originating from artificial errors. This Hamiltonian is similar to what accelerator researchers have frequently assumed for theoretical studies of space-charge effects in AG beam transport [3].

¹Gilson, Davidson, and their coworkers of Princeton Plasma Physics Laboratory also constructed a linear Paul trap for beam physics purposes. Their trap geometry is not the most popular four-rod type but a cylinder consisting of four 90-degree azimuthal sectors. The system is referred to as “PTSX” (Paul Trap Simulator Experiment) that has produced fruitful experimental results for the last decade [11–13].

²S.L. Sheehy, private communication.

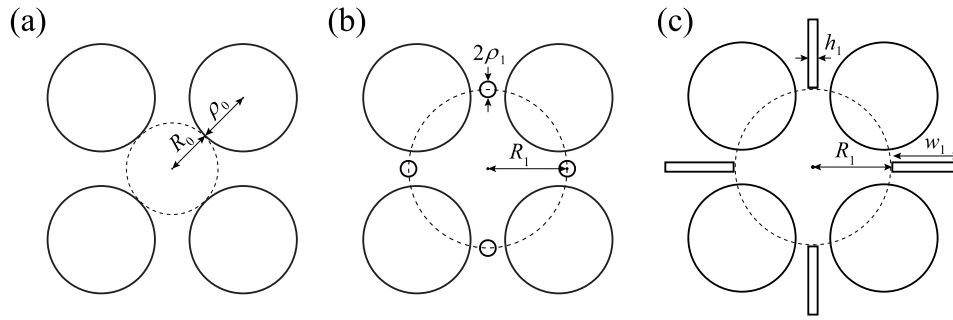


Fig. 1 Cross sectional views of linear Paul traps. (a) regular Paul trap, (b) a modified Paul trap with extra multipole rods of radius ρ_1 , (c) a modified Paul trap with extra planar electrodes of thickness h_1 and width w_1 . The minimum distance from the trap axis to the quadrupole electrodes' surfaces is denoted as R_0 while R_1 stands for the distance to either (b) the center of each extra rod or (c) the edge of each extra plate.

While the weak potential δV is usually ignored in standard textbooks [14], it does exist in a real trap, enhancing nonlinear resonances under certain conditions. Such a nonlinear potential is also present in any particle accelerator that always has finite mechanical imperfections and even nonlinear multipole magnets for beam orbit correction [1]. In a linear Paul trap, the main source of δV is the misalignments of the quadrupole rods. The non-hyperbolic surfaces of the rods can be another source of weak nonlinearity. In any case, the quadrupole electrodes give rise to not only the linear focusing potential but also the nonlinear perturbing potential. This means that it is impossible to control the strength of δV independently of the focusing field. In an accelerator, the time structures of $K(\tau)$ and $\delta V(\tau)$ are not necessarily identical; there is no direct correlation between these two functions especially when $\delta V(\tau)$ comes from correction magnets.

The purpose of this paper is to show a possible design of a multipole ion trap optimized for a wider range of beam dynamics studies than the regular Paul trap [15]. The proposed modified Paul trap has extra electrodes that enable us to control the strengths and time structures of low-order nonlinear fields separately from the linear focusing potential. We employ the ‘‘Warp’’ code throughout this design study to analyze the multipole field in the trap [16]. Although Warp is known as a Particle-In-Cell simulation code, it also has the function of an efficient Poisson solver. We here numerically seek for the best conceptual design of the multipole trap, clarifying the dependence of nonlinear-field components on the electrode geometry.

2. Extra Electrodes for Nonlinear-Field Excitation

The cross sectional view of a typical linear Paul trap is sketched in Fig. 1 (a). An AG focusing potential is provided by applying proper rf voltages to the four electrode rods. Each pair of the electrodes facing each other across the trap axis usually has an identical rf potential while the signs of the voltages on neighboring electrodes are re-

versed. Ideally, these electrodes should have a hyperbolic surface to produce a pure quadrupole field, but we mostly adopt a simple circular column for the sake of manufacturing easiness. This practical simplification results in weak distortion of the linear rf potential; namely, nonlinear components inevitably appear in the plasma confinement field, depending on the size of the electrode rods. In order to minimize the nonlinearity, the radius ρ_0 of each rod is chosen to satisfy the condition $\rho_0/R_0 \approx 1.15$ where R_0 is the radius of the trap aperture [17]. In the Paul traps currently used for S-POD, $R_0 = 5$ mm and thus $\rho_0 = 5.75$ mm. The nominal operating frequency is 1 MHz at which the maximum rf amplitude required for the full tune-space survey is only less than ~ 100 V. In the following numerical calculations with the Warp code, we simply assume these numbers without loss of generality³.

Nonlinearity of lower order affects the beam behavior more seriously unless we intentionally enhance higher-order fields for a certain purpose. The sextupole and octupole nonlinearities are of particular importance not only because their orders are the lowest and second lowest but also because they are often used for beam orbit correction. The multipole trap must have an ability to control these nonlinearities. The most straightforward way for this goal is to increase the number of electrodes. Considering that δV is much weaker than the quadrupole potential in any particle accelerators, we better keep the standard Paul-trap configuration in Fig. 1 (a) and just add supplemental electrodes for nonlinear-field excitation. The extra electrodes should be small to avoid too strong distortion to the linear focusing field. Since our chief concern is the controllability of sextupole and octupole nonlinearities, four extra poles will suffice. The shape of these poles is not necessarily cylindrical as shown in Fig. 1 (b) but would rather be a flat plate for some practical reasons. In fact, it is difficult to hold a long tiny rod precisely.

When $R_0 = 5$ mm, two neighboring quadrupole rods are distanced only by 3.7 mm. Note also that we usu-

³Note that everything scales as long as the ratio ρ_0/R_0 is fixed.

ally use an electron beam to ionize neutral atoms within the trap aperture for plasma production. Since electrons from an e-gun go through the narrow space in between the quadrupole rods, too thick an extra electrode is not acceptable. The diameter of the supplemental rods in Fig. 1 (b) should then preferably be a millimeter or even smaller. Such a thin wire may easily bend, worsening the longitudinal uniformity of the plasma confinement field. From these technical considerations, we here adopt the trap geometry as illustrated in Fig. 1 (c). It is actually easier to insert and fix a thin plate rather than a thin wire. The thickness and radial width of the four planar electrodes are denoted by h_1 and w_1 , respectively. Each plate is symmetrically set the distance R_1 away from the trap axis. R_1 must be greater than the aperture radius R_0 ; otherwise, the number of ions we can confine in the trap is considerably reduced due to collisions with the plates. These extra plates are electrically isolated from each other, so that we can apply arbitrary rf voltages generated by independent power sources. For completeness, a brief description of the trap geometry in Fig. 1 (b) is given in Appendix.

3. Optimization of the Planar Electrodes

The rf wavelength at the typical S-POD operating frequency f_{rf} of 1 MHz is roughly 300 m, much greater than the overall dimension of the Paul trap. We can thus employ the static-field approximation to analyze the transverse multipole fields with a specific design of electrodes. The scalar potential ϕ_{rf} of the plasma confinement field can be expressed as $\phi_{\text{rf}}(x, y, t) = F(x, y)T(t)$ where $F(x, y)$ satisfies the Laplace equation whose general solution written with the polar coordinates (r, θ) is

$$F(r, \theta) = \sum_{n=1}^{\infty} a_n \left(\frac{r}{R_0} \right)^n \cos(n\theta + \varphi_n), \quad (2)$$

with a_n and φ_n being constant parameters. In a standard sinusoidal excitation of the quadrupole electrodes, the time-dependent part is simply given by $T(t) = \cos(2\pi f_{\text{rf}}t + \text{const.})$. In beam physics applications, $T(t)$ is generally a periodic step function whose waveform emulates the discrete lattice structure of a particular machine. The quadrupole focusing potential in Eq. (1) corresponds to the $n = 2$ term in Eq. (2). The second multipole coefficient a_2 is, therefore, much larger than any other coefficients. A question now is how to control the coefficients of the sextupole ($n = 3$) and octupole ($n = 4$) terms by using the planar electrodes.

3.1 Suppression of nonlinear multipole components

The applicability of the S-POD system to various experimental purposes ought to be maintained even after a regular four-rod-type trap is replaced by the modified multipole trap. The potential δV must be weakened rather than

enhanced when we wish to explore any beam dynamic effects where nonlinear driving forces are of no substantial importance. Conveniently, the extra electrodes are usable to improve the linearity of the plasma confinement field despite that they are originally introduced for nonlinearity enhancement. In an ideal Paul trap with no fabrication errors and no extra electrodes, a_6 is the lowest nonlinear coefficient that inevitably appears due to the symmetry of the trap structure. As mentioned above, we can minimize the magnitude of a_6 by requiring $\rho_0/R_0 \approx 1.15$. The ratio a_6/a_2 can then be made on the order of 10^{-4} . The planar electrodes shown in Fig. 1 (c) can further reduce this ratio if we carefully choose their radial position and thickness.

If these extra plates are infinitely thin and inserted precisely in the middle of two neighboring quadrupole rods, they do not disturb the original electric field as long as they are grounded. That is obvious because the existence of such grounded plates has no influence on the boundary condition imposed by the original Paul-trap geometry. In reality, the plate thickness is finite, which distorts the original electric field and enhances a_6/a_2 . Since the plates cannot be too thin from the viewpoint of precision machining and alignment, we here assume $h_1 = 1$ mm for example. We also assume temporarily that the plates are very wide ($w_1 \rightarrow \infty$). Figure 2 (b) shows the ratio a_6/a_2 plotted as a function of the radial position R_1 of the plates. a_6 has been completely eliminated at $R_1 \approx 8.5$ mm. It is always possible to find a similar operating condition for a different choice of h_1 . The optimum value of R_1 at which a_6 vanishes fulfills the simple scaling law

$$\frac{R_1}{R_0} = 1.948 + 0.153 \log \frac{h_1}{R_0}, \quad (3)$$

under the condition $\rho_0/R_0 = 1.15$.

We reasonably expect that this conclusion will approximately hold even if the plate width w_1 is finite. The position of the inner edge, namely, R_1 is definitely important, but on the other hand, the outer edge must have only little effect on the field within the trap aperture unless w_1 is too small. We have confirmed that in the present case, the aperture field is insensitive to w_1 if it exceeds about 4 mm. In the following discussion, therefore, we ignore the effect of the outer edge for simplicity, assuming that w_1 has been chosen sufficiently large.

3.2 Octupole control mode

We now investigate how to control low-order nonlinear components. It is easy to strengthen the octupole ($n = 4$) nonlinearity because the modified trap has four extra poles. a_4 can be made larger by applying equal potentials to the planar electrodes. Every four multipole components (a_4, a_8, a_{12}, \dots) are then generated due to the symmetry of the boundary condition, but a_4 is much greater than other coefficients. The solid curves in Fig. 3 (a) represent the equipotential lines when an identical voltage V_0 is given to each plate. Figure 3 (b) indicates the relative octupole

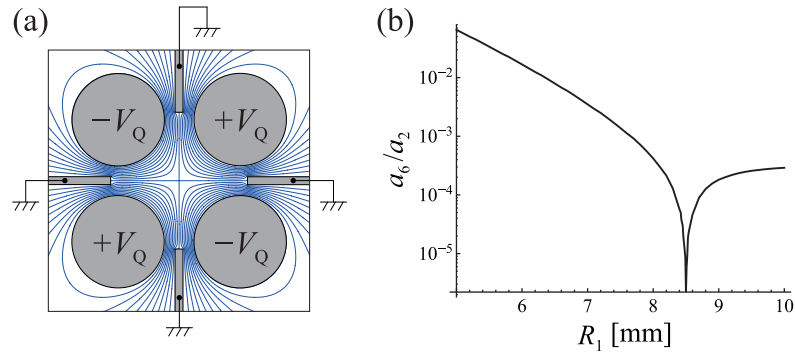


Fig. 2 Electrodes' potentials in the normal operating mode where low-order nonlinearities are minimized. The left panel shows the equipotential lines when all four extra plates are grounded. The voltages of quadrupole symmetry are given to the four circular rods for transverse ion confinement. The R_1 -dependence of the ratio a_6/a_2 is plotted in the right panel, assuming that $h_1 = 1$ mm.

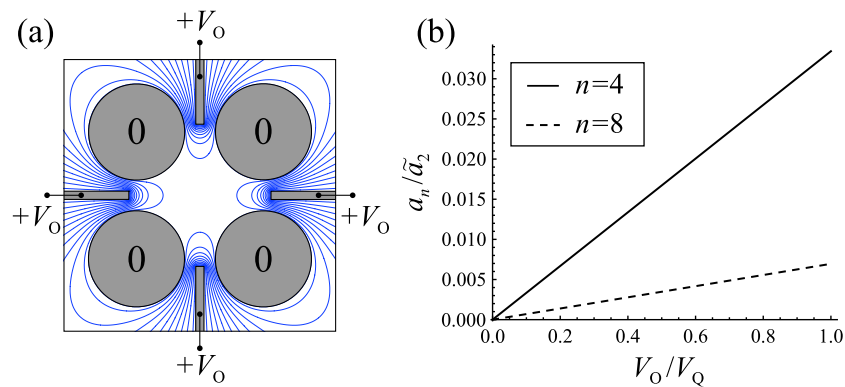


Fig. 3 Electrodes' potentials in the octupole control mode. The left panel shows the equipotential lines when the four planar electrodes are given equal voltages V_0 . All four quadrupole rods are grounded. The right panel shows the octupole strength a_4 normalized by \tilde{a}_2 , i.e. the quadrupole strength of the normal operating mode when $V_0/V_Q = 1$. The plate thickness is chosen to be $h_1 = 1$ mm. For reference, a_8/\tilde{a}_2 is also plotted with a broken line.

strength achievable with the potential configuration in the left panel. a_4 is normalized by the quadrupole strength \tilde{a}_2 in the normal operating mode shown in Fig. 2 (a)⁴. The abscissa stands for the voltage ratio V_0/V_Q . The normalized magnitude of a_8 is also plotted for reference. When V_0 is comparable to the linear focusing voltage V_Q , the magnitude of the octupole coefficient becomes a few percent of \tilde{a}_2 . This level of fourth-order nonlinearity is more than enough for a systematic study of octupole imperfection effects in a particle accelerator. The octupole field can be further strengthened by the use of thinner plates if necessary. According to Warp calculations, a_4 scales as $a_4/\tilde{a}_2 \approx 0.0166 \times (h_1/R_0)^{-0.441}$ when $V_0/V_Q = 1$.

The strengths of nonlinear components are almost unchanged even if we excite the quadrupole rods simultaneously with the planar electrodes. The total electric field when the quadrupole rods also have the finite voltages $\pm V_Q$

is simply the superposition of the field in Fig. 2 (a) and that in Fig. 3 (a). This is because the sum of these two independent fields satisfies the same boundary condition as the total field has to do. Suppose that there are N independent electrodes of arbitrary cross sections fixed at certain transverse positions. Each electrode is assumed to have a constant voltage V_i ($i = 1, 2, \dots, N$). The total static potential generated by these electrodes can be decomposed into N terms as $F(x, y) = \sum_{i=1}^N \psi_i(x, y)$ where ψ_i is the scalar potential derived from the Laplace equation under the boundary condition that all electrodes except for the i -th one are grounded. This is evident because the sum $\sum_{i=1}^N \psi_i$ is still a solution to the Laplace equation and satisfies the proper boundary condition.

3.3 Sextupole control mode

The effective excitation of the sextupole field is a bit tricky. Unlike the octupole control mode in Fig. 3 (a), we need to add finite voltages not only to the planar electrodes but also to the quadrupole rods. Figure 4 (a) shows an example of the boundary condition that allows us to en-

⁴In the following, we use the notation \tilde{a}_2 for the quadrupole strength under the *normal operating condition* (Fig. 2) to distinguish it from a_2 of other operating modes; \tilde{a}_2 is identical to a_2 of the normal operating mode with V_Q equalized either to V_0 in Fig. 3 or to V_S in Fig. 4. Note that a_2 is zero in the nonlinearity control modes without electrodes' misalignments.

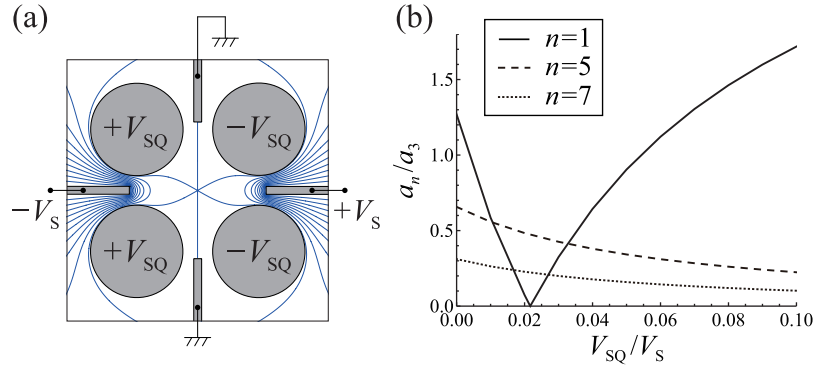


Fig. 4 Electrodes' potentials in the sextupole control mode. The left panel shows the equipotential lines when the voltages $\pm V_{SQ}$ and $\pm V_S$ are applied to the quadrupole and horizontal planar electrodes for sextupole enhancement. The strengths of other low-order multipole components relative to the sextupole strength are plotted in the right panel as a function of the voltage ratio V_{SQ}/V_S . The plate thickness is chosen to be $h_1 = 1$ mm.

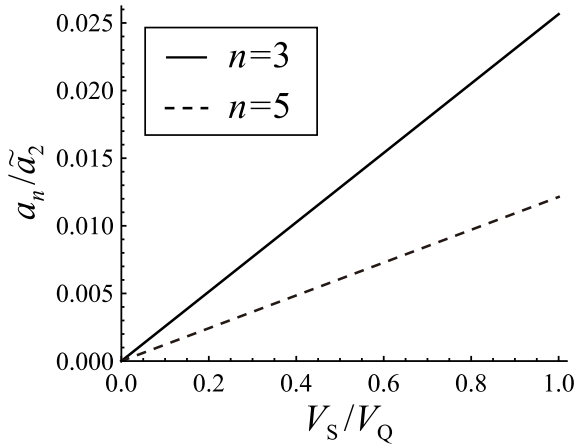


Fig. 5 Strengths of sextupole ($n = 3$) and decapole ($n = 5$) fields vs. the potential ratio V_S/V_Q in the sextupole control mode. V_{SQ} has been adjusted to the optimum value required by the condition (4) to eliminate the dipole component a_1 . The coefficients a_3 and a_5 are normalized by the quadrupole strength \tilde{a}_2 evaluated under the normal operating condition with $V_Q = V_S$.

large the coefficient a_3 . The potentials V_S of opposite signs are given to the horizontal plates while the vertical pair is grounded. In addition to $\pm V_S$, we apply the voltages $\pm V_{SQ}$ to the quadrupole rods as depicted. This electrode excitation pattern gives rise to every other multipole components. Particular attention must be paid to the dipole component a_1 because its order is the lowest. Fortunately, a_1 can be minimized in the vicinity of the trap's mechanical center by adjusting the ratio V_{SQ}/V_S . As is clear from Fig. 4 (b), the dipole component disappears when $V_{SQ}/V_S \approx 0.02$. The optimum voltage ratio required for the minimization of a_1 obeys the scaling law

$$\frac{V_{SQ}}{V_S} \approx 1.048 \times \left(\frac{h_1}{R_0}\right)^{-0.455}, \quad (4)$$

if the quadrupole rods are designed to satisfy the condition $\rho_0/R_0 = 1.15$ and the four plates are fixed at the radial positions defined by Eq. (3).

The strengths of the sextupole ($n = 3$) and decapole ($n = 5$) components divided by the quadrupole strength \tilde{a}_2 in the normal operating mode are evaluated in Fig. 5 under the condition in Eq. (4). By increasing V_S to the same level of V_Q , a_3 becomes a few percent of \tilde{a}_2 . We have also found how these nonlinearities scale as a function of the plate thickness h_1 . Provided that V_{SQ}/V_S satisfies the condition (4), the relative strengths follow the scaling laws $a_3/\tilde{a}_2 \approx 0.0135 \times (h_1/R_0)^{-0.454}$ and $a_5/\tilde{a}_2 \approx 0.0064 \times (h_1/R_0)^{-0.456}$ where we have assumed $V_Q = V_S$ as an example. Interestingly, the three ratios V_{SQ}/V_S , a_3/\tilde{a}_2 and a_5/\tilde{a}_2 have roughly the same power dependence on the geometric factor h_1/R_0 .

4. Discussion

4.1 Effect of electrode misalignments

It is important to figure out how the ideal multipole fields calculated in the last section are affected by the misalignments of the electrodes. Such an artificial error is unavoidable in practice, which results in considerable enhancement of all nonlinear fields. To check this error-induced effect, we randomly shift all electrodes about the ideal positions, and then, expand the resultant electric field into multipole components. Table 1 summarizes the relative multipole strengths (%) in various operating modes explained in the last section. "Regular Paul trap" has the ordinary four-rod structure illustrated in Fig. 1 (a). The "normal operating mode" corresponds to the electrode excitation pattern in Fig. 2(a) where all extra plates are grounded. We have assumed that V_S in the "sextupole control mode" and V_Q in the "octupole control mode" are equal to V_Q in the "normal operating mode". V_{SQ} in the "sextupole control mode" is automatically determined from Eq. (4) once we choose V_S . The normalization con-

Table 1 Multipole strengths in various operating modes. The multipole coefficients normalized by the quadrupole strength \bar{a}_2 (normal operating mode) are indicated in percent. It has been assumed that $V_S = V_Q$ in the sextupole control mode and $V_O = V_Q$ in the octupole control mode. The aperture size $R_0 = 5$ [mm], which determines the optimum radius of the quadrupole rods to be 5.75 [mm]. The thickness of the planar electrodes has been fixed at $h_1 = 1$ [mm]. The multipole expansion is carried out about the electric-field center (where $a_1 = 0$) defined in the normal operating mode. The dipole component then becomes non-zero in the sextupole and octupole control mode because the location of the field center slightly shifts when finite voltages are applied to the misaligned plates.

		a_1/\bar{a}_2	a_2/\bar{a}_2	a_3/\bar{a}_2	a_4/\bar{a}_2	a_5/\bar{a}_2	a_6/\bar{a}_2	a_7/\bar{a}_2	a_8/\bar{a}_2
Regular Paul trap	No error	0	100	0	0	0	0.032	0	0
	Case I	0	100	0.358	0.125	0.065	0.038	0.011	0.013
	Case II	0	100	0.715	0.251	0.130	0.056	0.021	0.027
Multipole trap (normal operating mode)	No error	0	100	0	0	0	0	0	0
	Case I	0	100	0.358	0.125	0.071	0.029	0.014	0.016
	Case II	0	100	0.716	0.250	0.143	0.058	0.029	0.033
Multipole trap (sextupole control mode)	No error	0	0	2.565	0	1.213	0	0.570	0
	Case I	0.093	0.074	2.567	0.054	1.215	0.026	0.571	0.010
	Case II	0.185	0.148	2.571	0.108	1.216	0.052	0.572	0.019
Multipole trap (octupole control mode)	No error	0	0	0	3.343	0	0	0	0.695
	Case I	0.135	0.087	0.106	3.349	0.051	0.032	0.030	0.697
	Case II	0.269	0.174	0.212	3.349	0.102	0.064	0.060	0.697

stant \bar{a}_2 is evaluated under the boundary condition of the normal operating mode. Note that the centroid of an ion plasma in the trap is located at the multipole-field center where the dipole component vanishes. We, therefore, need to expand the scalar potential about the field center (instead of the original mechanical center) to make a reasonable estimate of a_n . We have here defined the field center under the boundary condition of the normal operating mode because the plasma is exposed to this strong focusing potential most of the time. The possible error-induced shift of the field center is on the order of 0.1 mm at most even with relatively large electrodes' misalignments. This number is much smaller than the aperture size of 5 mm. As the transverse extent of an ion plasma confined in our trap is typically around 1 mm in radius, no extra ion losses will occur due to such a tiny shift of the plasma centroid.

The multipole coefficients in Table 1 are obtained by averaging a hundred independent Warp data based on a hundred different sets of random numbers to define the electrode positions. The quadrupole and planar electrodes are misaligned simultaneously. Two different sizes of root-mean-squared (rms) errors, i.e. 50 μm (Case I) and 100 μm (Case II), are considered in the table. As expected, all multipoles have been excited by the misalignments. The standard deviation of an error-induced multipole coefficient calculated from the one hundred samples is somewhat smaller than its central value listed in the table. The rms shifts of the plasma centroid are 31 μm for Case I and

63 μm for Case II. It is quite reasonable that the nonlinear fields become stronger on average as the rms alignment error increases. We recognize from the data in Table 1 that the magnitudes of low-order multipole coefficients grow almost linearly with respect to the rms error size. A practically important fact is that the introduction of the four extra plates does not deteriorate the field quality of the original Paul trap without the plates. The strengths of low-order nonlinear components caused by the error are insensitive to whether we add the four misaligned plates or not.

It is informative to point out that the extra electrodes may be utilized to reduce the low-order error-induced nonlinear fields in the normal operating mode. a_3/\bar{a}_2 is typically on the order of 0.1% as suggested in Table 1. This unwanted third-order component can be suppressed strongly by superimposing proper low voltages to all electrodes. These additional voltages for error-induced sextupole minimization are decomposed into two specific potential configurations; one is the configuration in Fig. 4 (a) and the other the skew sextupole configuration obtained by rotating Fig. 4 (a) by 90 degrees around the axis. Since the ratio V_{SQ}/V_S satisfies Eq. (4), we have only two free parameters, i.e. the voltage V_S in each configuration, to be adjusted. The optimum values of V_S 's can be determined easily if the size and direction of each electrode's misalignment are known. Such information about actual mechanical errors is indeed unknown, but we can at least measure the ion-loss rate due to sextupole resonance with many different combi-

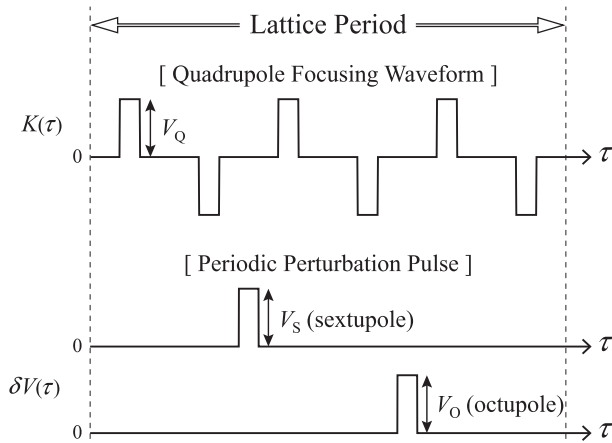


Fig. 6 An example of the rf waveform emulating a FODO beam transport channel. The quadrupole filling factor is chosen to be 0.25. The lower picture indicates the timing when the octupole potential (V_O) in Fig. 3 (a) or the sextupole potential (V_S and V_{SQ}) in Fig. 4 (a) is switched on for non-linearity enhancement. Each nonlinear perturbation pulse is excited every three FODO periods. The widths of all pulses are taken identical.

nations of the additional voltages⁵. The data of systematic ion-loss measurements enable us to find the optimum V_S 's for sextupole minimization. Those data also tell us how much mechanical errors are actually contained in the trap.

4.2 Tracking simulation tests

A major advantage in S-POD experiment is the high flexibility of the focusing function $K(\tau)$ in Eq. (1). In a particle accelerator, the lattice design uniquely determines the form of $K(\tau)$. If we wish to explore beam dynamics in a different lattice, we must construct another large-scale machine. By contrast, $K(\tau)$ can be modified over a wide range in S-POD because the rf voltages applied to the electrodes determine the external driving potential, in other words, this is just a matter of the electronics system. In the multipole ion trap, $K(\tau)$ is proportional to the quadrupole voltage V_Q in Fig. 2 (a). The upper picture in Fig. 6 represents a typical rf waveform for V_Q imitating a so-called ‘‘FODO’’ channel. The rf power supply system developed for S-POD can readily produce much more complex waveform if necessary.

The extra planar electrodes of the multipole trap make it feasible for us to introduce a nonlinear periodic perturbation independently of the main focusing waveform. In the case of Fig. 6, the plates are excited every three FODO

cells (the lower picture); namely, the period of $\delta V(\tau)$ in Eq. (1) is chosen three times longer than that of $K(\tau)$. This kind of situation commonly takes place in a circular machine where a small number of nonlinear magnets are added for beam orbit correction. Since the periodicities of the linear and nonlinear driving forces are different, we expect additional resonance stop bands to appear, depending on how often we turn on the nonlinear perturbation. In the present example, the nonlinearity of a particular order ($n = 3$ or 4) is considerably enhanced every three FODO periods. The stability threshold of the bare betatron tune ν_0 per lattice period is then $1.5 (= 0.5 \times 3)$. At zero beam intensity, the well-known incoherent resonance condition can be written as $n\nu_0 = m$ [1] where n is the order of resonance, and m is a positive integer. We have assumed here that the horizontal tune ν_x and the vertical tune ν_y are equal, i.e. $\nu_x = \nu_y = \nu_0$, for the sake of simplicity while it is possible in S-POD to separate the two transverse tunes.

We performed test numerical simulations with the Warp code to verify the resonance condition, incorporating the detailed multipole field distributions evaluated in the previous sections. The time evolution of the rms emittance of an ion plasma in the multipole trap was computed assuming the rf waveform in Fig. 6. The emittance growth rates after a hundred FODO cells are plotted in Fig. 7 as a function of the bare tune ν_0 . The solid line in each panel is obtained from Warp simulations in the absence of electrode alignment errors, while the broken line shows a typical case where all electrodes are randomly shifted by the rms average of $100 \mu\text{m}$. The repetition frequency of a FODO waveform is set at 1 MHz, so the hundred cells correspond to $100 \mu\text{s}$ in an actual experiment. Figure 7 (a) shows the Warp output obtained under the normal operating condition. We confirm that in the absence of the perturbation pulse, no resonance occurs over the whole tune range because the external force is perfectly linear in the modified trap without electrode misalignments (see Table 1). Serious instability can, however, be identified near $\nu_0 = 1$ when the electrodes are misaligned. This is due to the third-order resonance (the lowest-order nonlinearity) caused by the imperfection field. No other stop bands of higher order resonances are visible within a hundred FODO periods, except for a very weak fourth-order instability at $\nu_0 = 3/4$. Needless to say, the emittance growth rate depends on how the electrodes are misaligned. In this simulation, we have shifted all eight electrodes so that the averaged multipole coefficients of Case II (normal operating mode) in Table 1 are approximately reproduced.

Once the perturbation pulse is excited, the emittance growth picture becomes essentially different. Figure 7 (b) represents the case where the sextupole potential in Fig. 4 (a) is periodically switched on. The pulse height of the perturbation wave has been adjusted to satisfy $V_S = V_Q$ in each simulation. We observe clear instabilities at $3\nu_0 = m$, no matter whether the misalignments are finite. The emittance behavior is changed to Fig. 7 (c)

⁵Experimental simulations of intense beam dynamics by means of the S-POD system are far faster than any multi-particle computer simulations. An ion-loss measurement based on a particular AG focusing waveform is completed typically within ten seconds, regardless of the plasma density. In addition, the whole experimental process is automated, so we do not have to stay beside S-POD to retune fundamental parameters. Even if we execute a hundred independent measurements at a hundred different operating points, that takes only less than 17 minutes.

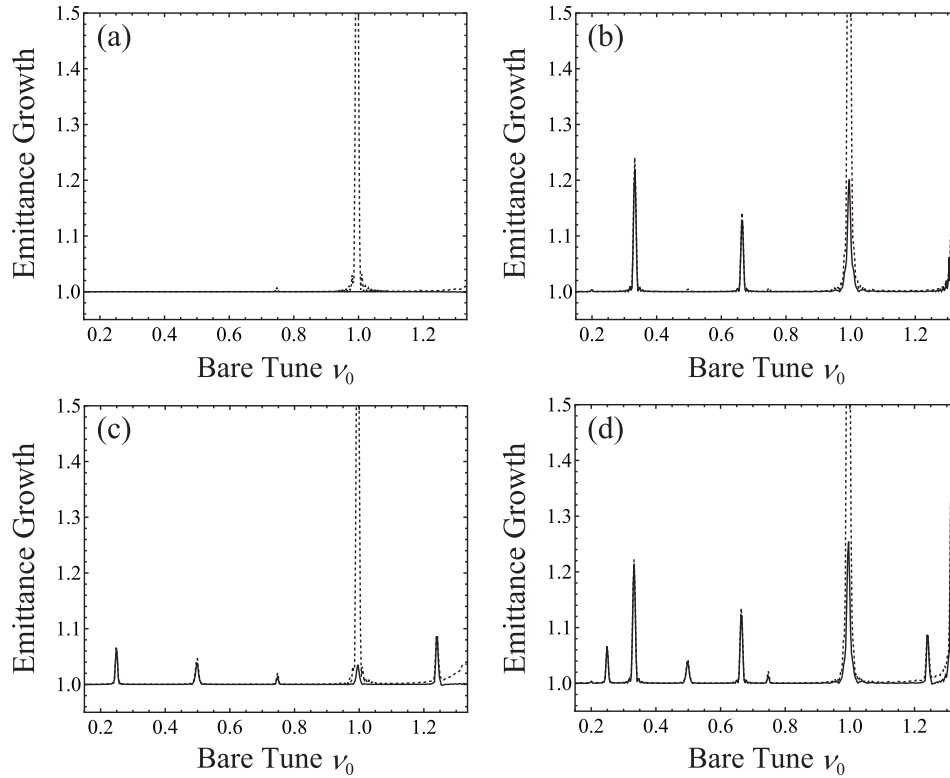


Fig. 7 Warp simulation results assuming the time structures of $K(\tau)$ and $\delta V(\tau)$ in Fig. 6. The rms emittance growth rates after 100 FODO periods are plotted as a function of bare betatron tune ν_0 . The Coulomb self-field potential has been ignored in these simulations. The panel (a) is the result under the normal operating condition where no perturbation pulse is excited. Other three panels correspond to the cases where we periodically switch on (b) only the sextupole pulse under the condition $V_s = V_Q$, (c) only the octupole pulse under the condition $V_O = V_Q$, and (d) both sextupole and octupole pulses.

by applying the octupole pulses instead of the sextupole pulses. We now observe small peaks at $4\nu_0 = m$ due to the fourth-order resonance. Figure 7 (d) shows what happens when both sextupole and octupole perturbations are activated. Naturally, stop bands are generated at $3\nu_0 = m$ and $4\nu_0 = m$.

It is also possible to selectively drive only one sextupole or one octupole resonance at a specific tune. For this purpose, we use a sinusoidal waveform for $\delta V(\tau)$ instead of a stepwise pulse as in Fig. 6. The frequency of the sinusoidal perturbation has to be matched to that of a proper Fourier harmonic of the original periodic pulse.

5. Summary

We have proposed a simple design of a multipole ion trap dedicated to fundamental beam-physics experiments with the S-POD system. The modified Paul trap has four extra electrodes in between the regular quadrupole rods, which control low-order nonlinearities in the plasma confinement potential. From a practical point of view, we focused our discussion on the insertion of thin metallic plates. An efficient Poisson solver was employed to study the dependence of the aperture field on the electrode geometry. It has been shown that the sextupole and oc-

tupole driving fields can be enhanced independently of the quadrupole focusing potential. In the so-called normal operating mode (Fig. 2), the modified trap operates just like an ordinary linear Paul trap; the field linearity can even be improved by placing the extra plates at the optimum positions defined by Eq. (3). The octupole field can be strengthened at an arbitrary moment simply by applying the same voltages to the four plates (Fig. 3). In the sextupole control mode, we excite the planar electrodes and quadrupole rods simultaneously in such a way as illustrated in Fig. 4. The applied voltages are chosen to minimize the dipole component according to Eq. (4).

When the electrodes are shifted from their ideal positions due to mechanical imperfections, all higher order components become finite. Such error-induced multipole fields are, however, sufficiently weak as long as the electrode misalignments are within a reasonable level. As shown in Table 1, the four extra plates newly introduced for nonlinearity control do not affect the field quality of the original Paul trap. Numerical simulations actually demonstrate that we can create the third- and/or fourth-order stop bands at specific tunes without enhancing unwanted resonances of other orders. The present design of a multipole ion trap thus widens the range of beam dynamics experiments we can do with the S-POD system. In particular,

the stability of intense hadron beams in a variety of non-linear lattices can be explored experimentally and much more quickly than any numerical simulations.

On the basis of this design study, we are now planning to construct a multipole ion trap for S-POD. The nominal operating frequency will be set at 1 MHz, the same as the existing Paul traps at Beam Physics Laboratory of Hiroshima University. The aperture radius R_0 is 5 mm, and then, the radius ρ_0 of the quadrupole rods has to be 5.75 mm. The thickness h_1 of the four extra plates is probably chosen 1 mm or less. In case $h_1 = 1$ mm, the inner edge of each plate is fixed 8.5 mm away from the trap axis, according to Eq. (3). The plate width w_1 should be greater than at least about 5 mm, so that the effect of the outer edge on the aperture field becomes negligible. Under these mechanical conditions, the sextupole and octupole strengths can be increased to a few percent of the dominant quadrupole strength with a perturbation voltage (V_S or V_O) of lower than about 100 V. The required perturbation voltage can be further lowered, if necessary, by using thinner plates⁶. In any case, we only need minor modifications to the current power-supply system of S-POD for future experimental studies of intense beam dynamics with the modified Paul trap.

Acknowledgments

This work is supported in part by JSPS KAKENHI Grant Number 15H03662. One of the authors (KF) is indebted to Dr. K. Ito for valuable discussion.

Appendix. Extra Electrodes of a Cylindrical Shape

The basic feature of the multipole field within the trap aperture does not essentially change even if we replace the planar electrodes in Fig. 1 (c) by the small circular rods in Fig. 1 (b). Apart from a technical question of which trap geometry is easier to fabricate, the electric-field properties of both designs turn out to be very similar to each other. First of all, a_6 can be eliminated in the normal operating mode by adjusting the radius ρ_1 of the extra rods. The scaling law in this case is given by

$$\frac{R_1}{R_0} = 2.162 + 0.225 \log \frac{\rho_1}{R_0}, \quad (\text{A.1})$$

instead of Eq. (3). In the octupole control mode, we simply

apply an identical voltage V_O to all four extra rods just like the previous case in Fig. 3 (a). When V_O is set equal to the quadrupole focusing voltage V_Q on the main rods, the octupole coefficient a_4 relative to the dominant quadrupole coefficient \tilde{a}_2 scales as $a_4/\tilde{a}_2 \approx 0.0153 \times (\rho_1/R_0)^{-0.558}$. It is also possible in the sextupole control mode to minimize the dipole component near the trap axis. The optimum ratio of V_{SQ} and V_S for dipole suppression can be determined from the scaling law $V_{SQ}/V_S \approx 0.963 \times (\rho_1/R_0)^{-0.577}$.

- [1] A.W. Chao, M. Tigner (Eds.), *Handbook of Accelerator Physics and Engineering* (World Scientific, Singapore, 1999) and references therein.
- [2] See, e.g., Proceedings of the 54th ICFA Advanced Beam Dynamics Workshop on High-Intensity, High-Brightness and High-Power Hadron Beams (Michigan, USA, 2014).
- [3] M. Reiser, *Theory and Design of Charged Particle Beams* (John Wiley & Sons, New York, 2008) and references therein.
- [4] H. Okamoto and H. Tanaka, Nucl. Instrum. Methods A **437**, 178 (1999).
- [5] R. Takai, H. Enokizono, K. Ito, Y. Mizuno, K. Okabe and H. Okamoto, Jpn. J. Appl. Phys. **45**, 5332 (2006).
- [6] S. Ohtsubo, M. Fujioka, H. Higaki, K. Ito, H. Okamoto, H. Sugimoto and S.M. Lund, Phys. Rev. ST Accel. Beams **13**, 044201 (2010).
- [7] H. Takeuchi, K. Fukushima, K. Ito, K. Moriya, H. Okamoto and H. Sugimoto, Phys. Rev. ST Accel. Beams **15**, 074201 (2012).
- [8] H. Okamoto, M. Endo, K. Fukushima, H. Higaki, K. Ito, K. Moriya, S. Yamaguchi and S.M. Lund, Nucl. Instrum. Methods A **733**, 119 (2014).
- [9] K. Fukushima, K. Ito, H. Okamoto, S. Yamaguchi, K. Moriya, H. Higaki, T. Okano and S.M. Lund, Nucl. Instrum. Methods A **733**, 18 (2014).
- [10] K. Moriya, K. Fukushima, K. Ito, T. Okano, H. Okamoto, S.L. Sheehy, D.J. Kelliher, S. Machida and C.R. Prior, Phys. Rev. ST Accel. Beams **18**, 034001 (2015).
- [11] R.C. Davidson, H. Qin and G. Shvets, Phys. Plasma **7**, 1020 (2000).
- [12] E.P. Gilson, R.C. Davidson, P.C. Efthimion and R. Majeski, Phys. Rev. Lett. **92**, 155002 (2004).
- [13] E.P. Gilson *et al.*, Phys. Plasmas **20**, 055706 (2013).
- [14] P.K. Ghosh, *Ion Traps* (Oxford Science, Oxford, 1995) and references therein.
- [15] H. Okamoto, Y. Wada and R. Takai, Nucl. Instrum. Methods A **485**, 244 (2002).
- [16] D.P. Grote, A. Friedman, G.D. Craig, I. Haber and W.M. Sharp, Nucl. Instrum. Methods A **464**, 563 (2001).
- [17] D.R. Denison, J. Vacuum Sci. Technol. **8**, 266 (1971).

⁶Then, the optimum radial position of the inner edge comes closer to the aperture radius R_0 , according to Eq. (3).